

# The human posterior cingulate and the stress-response benefits of viewing green urban landscapes

Dorita H.F. Chang<sup>a,b,1</sup>, Bin Jiang<sup>c,d,1</sup>, Nicole H.L. Wong<sup>a</sup>, Jing Jun Wong<sup>a</sup>, Chris Webster<sup>e,\*</sup>,  
Tatia M.C. Lee<sup>a,b,\*</sup>

<sup>a</sup> Department of Psychology, The University of Hong Kong, Hong Kong

<sup>b</sup> The State Key Laboratory of Brain and Cognitive Sciences, The University of Hong Kong, Hong Kong

<sup>c</sup> Division of Landscape Architecture, Faculty of Architecture, The University of Hong Kong, Hong Kong

<sup>d</sup> Virtual Reality Lab of Urban Environments and Human Health, HKUrbanLabs, The University of Hong Kong, Hong Kong

<sup>e</sup> HKUrbanLabs, Faculty of Architecture, The University of Hong Kong, Hong Kong

## ARTICLE INFO

### Keywords:

Nature  
Green urban landscapes  
Stress  
Mental health  
fMRI

## ABSTRACT

The mechanistic and neural bases of why green environments drive positive mental health outcomes remain poorly understood. We show that viewing green urban landscapes that vary in terms of green-space density elicits corresponding changes in the activity of the human ventral posterior cingulate cortex that is correlated to behavioural stress-related responses. We further show that cingulate responses are engaged early in the processing cascade, influencing attentional and executive regions in a predominantly feedforward manner. Our data suggest a key role for this region in regulating (nature) dose-dependent changes in stress responses, potentially through its extensive connections to the prefrontal and hippocampal regions which in turn project towards the neuroendocrine system. As the posterior cingulate cortex is implicated in a variety of neurological diseases and disorders, these findings raise a therapeutic potential for natural environmental exposure, highlighting green-cover as a modifiable element that links to changes in limbic responses, and has health consequences for practitioners and city-planners alike.

## 1. Introduction

Work across a number of disciplines have converged to reveal that exposure to natural environments benefits mental health. For example, viewing rural images results in relatively more positive emotional states as compared to viewing images with urban content (Ulrich, 1981; Van den Berg et al., 2007). A short walk in a natural rather than urban setting reduces rumination behaviour (Bratman et al., 2015) and can improve mood and memory (Berman et al., 2012, 2008). Within urban contexts alone, self-perceived mental health is better for those living in greener versus less-green environments (Alcock et al., 2014). These findings align with still other work that indicate green environments, in addition to having obvious economic and environmental consequences, drive broad-reaching benefits including promoting better social ties, better self-discipline (Taylor et al., 2002), and can even result in accelerated recovery from surgery (Ulrich, 1984) and reduce crime (Kaplan, 1995; Schroeder, 2011). Still, the neural and mechanistic bases of why green environments drive positive mental health outcomes remain poorly understood. A limited body of imaging and psychobiological work have in-

dicated that exposure to natural environments modulates activity in prefrontal cortex (PFC) (Bratman et al., 2015; Park et al., 2007; Tost et al., 2019)– a region of the brain that serves broad executive functions, and activity in visuo-spatial and attention-related areas (Tang et al., 2017). As the previous reports involved coarse contrasts between exposure to natural- (e.g., forestry, mountains, water) vs urban-environments that differ in many respects sensorially, it is difficult to ascertain what it is in these environments that is key to driving both the reported psychological and neural modulations.

Using fMRI, we sought to reveal how green urban content (i.e., trees, bushes, grass) influences brain activity. Previous work has shown that the reported preference for particular landscapes, and the effectiveness of these scenes for promoting stress recovery scales differentially with green-space density (Jiang et al., 2016, 2015). In particular, behavioural preferences for urban landscapes increases with increases in green-space density until ~40%, after which preference ratings asymptote (Jiang et al., 2015). By contrast, following the induction of psychological stress, stress recovery appears to increase linearly with increases in green-space density (Jiang et al., 2016). Thus, we fathomed

\* Corresponding authors.

E-mail addresses: [cwebster@hku.hk](mailto:cwebster@hku.hk) (C. Webster), [tmcleee@hku.hk](mailto:tmcleee@hku.hk) (T.M.C. Lee).

<sup>1</sup> Both authors contributed equally to this work.

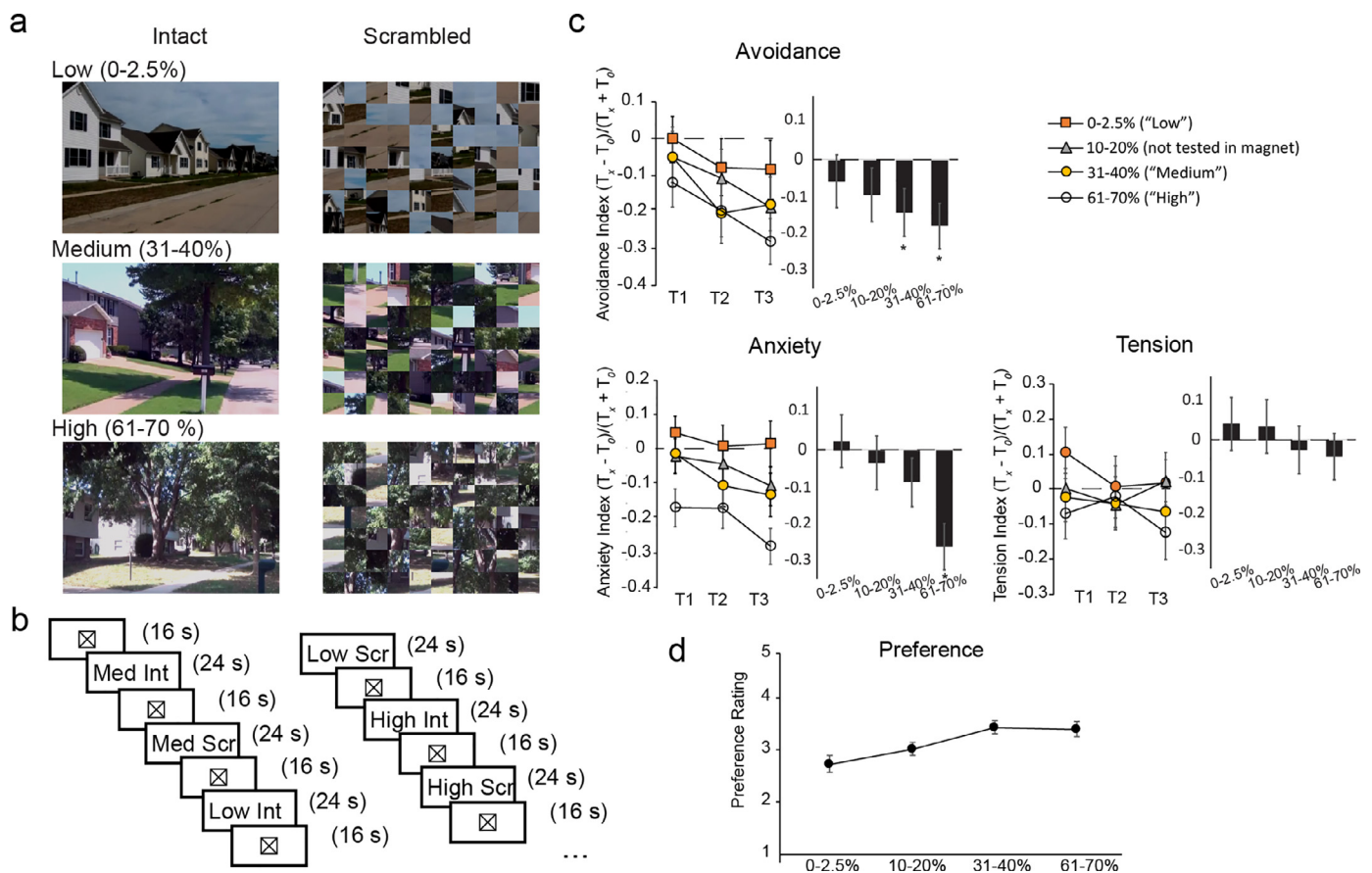


**Fig. 1.** (a) Sample stimuli from the three density levels tested in the fMRI. Stimuli were stereoscopic, and presented in the magnet using a prism setup. (b) Schematic of the structure of a sample scan run. Block order was pseudorandomized such that the intact block was always followed by the corresponding yoked-scrambled block. All blocks were interleaved with a fixation block carrying a modified nonius fixation to promote stable vergence. Each stimulus condition was repeated twice within one run. (c) Normalized mean ratings for each subscale of the VAS, and preference ratings across test blocks (left) and density conditions (right). Asterisks denote indices that are significantly different from zero. (d) Mean preference ratings across densities (higher is more preferred). Error bars represent  $\pm 1$  standard error of the mean.

that a good way to understand the functional benefits of viewing urban green space is to ask whether there are regions for which neural activity best matches behavioural dose-response profiles. As the prevalence of high-green-density environments is region-dependent, one might expect the potency of any effects driven by green space to be affected by the subject's historical exposure to such environments. For this reason, we tested exclusively East Asian participants who had not lived outside their place of origin for more than a one-month consecutive period.

We presented static three-dimensional images of neighborhood streets from various Midwestern metropolitan areas in the United States (Jiang et al., 2016, 2015). The streets varied in green-space density, defined as the number of pixels that were associated with trees versus those that were not, but were otherwise equated for luminance and chrominance. We chose to present images from three select densities: 0-2.5% (low), 31-40% (medium), and 61-70% (high), as previous work had indicated that these densities well capture characteristics of both changes in preference and stress ratings, with changes in green-space density.

Using fMRI, we first presented images in their intact or block-scrambled form (Fig. 1a) while participants completed a one-back task to maintain equivalent attentional demands across conditions. Within two-weeks of each scan, participants were again tested in the laboratory to attain self-reported stress and preference measures for the landscape images using the Visual Analog Scale – a widely used tool for rating perceived stress that has also been implemented in previous assessments of stress recovery responses (von Dawans et al., 2011), and a

landscape preference rating task. These behavioural measures were important for establishing that the static images were nonetheless effective in eliciting changes in stress and preference responses as demonstrated in previous work using lengthy, panning videos that are not well-suited for fMRI-testing (Jiang et al., 2016, 2015). Images were distinct from those presented for the fMRI so as to avoid potential repetition effects, and these tests were conducted after the fMRI session in order to avoid subject-demand characteristics.

Our questions were three-fold: Can we observe systematic changes in brain responses to parametric changes in green-space density within urban contexts alone? Further, can we relate behavioural-measures of stress-related and preference-related responses to green urban landscapes to neural responses? Finally, can we explore the architecture of the feedforward and feedback influences (i.e., effective connectivity) that are driven by the relevant regions of interest and observe modulations of connectivity based on green-space density? Based on previous work, we predicted that to the extent that viewing urban green landscapes has been shown to be beneficial to stress-relevant responses, and to the extent that stress-response benefits have been posited to involve mechanisms of attention, we may observe green-density-driven modulations of responses in key areas of the brain governing attention and stress regulation including parietal, prefrontal, insular, and even cingulate cortex, the last of which has been shown to be particularly relevant (Aguirre and D'Esposito, 1999; Kravitz et al., 2011; Vann et al., 2009; Wolbers and Büchel, 2005).

## 2. Methods

### 2.1. Participants

Forty-four observers (mean age of 23.7 years; 22 males) participated in this study. Participants had no history of neuropsychological disorders, had normal or corrected-to-normal vision as assessed by a linear acuity chart, and normal stereovision as assessed by the titmus stereotest. All participants were ethnically East Asian and had not lived outside their place of origin at any point for more than a one-month consecutive period. Participants provided written informed consent in line with ethical review and approval of the work by the ethics committee of the Human Research Ethics Committee, The University of Hong Kong. The data from three subjects (2 males) were excluded from final analyses due to extensive head movement.

### 2.2. Stimuli

Stimuli were static 3D images sampled from 3D videos captured by Jiang et al. (Jiang et al., 2016, 2015). Briefly, videos of neighborhood streets from various Midwestern metropolitan areas in the United States were captured with a Sony HMZ-T1 camera. The streets captured varied in green cover density, defined as the number of pixels that were associated with trees, bushes, and grass, versus those that were not, from 0-70% (for further specifics, see Jiang et al., 2016). In order to derive stimuli that could be suitably presented in the magnet, we selected 15 still frames (stimulus exemplars) from each video set depicting the three density levels: 0-2.5% (low), 31-40% (medium), 61-70% (high). This yielded a total of 45 unique images (15 per condition). Stimuli were presented in their veridical (intact) form, or were block-scrambled such that each block subtended  $.85 \text{ deg}^2$ . All images subtended  $8 \text{ deg} \times 6 \text{ deg}$  in size and were image-normalised such that each colour channel (RGB) within each image was matched in terms of their mean intensity. Further, image intensities were matched across stimuli. All stimuli were presented on a uniform black background.

For the in-laboratory behavioural tests, we tested an additional set of 15 images from a fourth density level (10-20%) in addition to those tested with the fMRI, in order to better capture dose-response characteristics. A different set of static images than those tested in the magnet were selected for the purpose the behavioural testing. Stimuli presented in the laboratory subtended  $26 \times 18 \text{ deg}$  in size.

### 2.3. Apparatus

Stimuli were viewed dichoptically in the magnet via a prism-setup (Schurger, 2009). Left and right eye images were presented concurrently (i.e., to the left and right of center) via an MR compatible LCD (Invivo Esys) placed at the back of the bore and controlled via custom protocols written in ePrime. Stimuli were viewed via a coil-mounted mirror via prism lenses (10 diopter prisms, base-out) mounted on custom MR-compatible frames. Frames were selected to match the subject's intrapupillary distance. Any additional optical correction needed (e.g., for myopia) was given via the addition of a second lens. Finally, left and right images were further segregated by means of a custom black drape placed in the middle of the bore, spanning its entire length, as well as an additional black cardboard divider placed on top of the headcoil, between the mirror and the coil (Schurger, 2009). Fusion was verified prior to the commencement of each session by presenting left and right calibration grids ( $6 \times 6 \text{ deg}$ ) that each contained an 'X' in its center. Participants were asked to ensure that these images were fused (i.e., report a single perceived image).

Dichoptic presentation of the stimuli for the behavioural, in-lab tests was done via a Shutter-presentation setup that consisted of a 144 hz monitor (27 inch Asus VG278) outfitted with an Nvidia 3D Vision 2 infrared emitter. Subjects viewed stimuli using corresponding shutter goggles at a distance of 50 cm as maintained by a chin-rest. In-lab tests

were presented via custom software written in Matlab (Mathworks) using extensions from Psychtoolbox (Brainard, 1997; Pelli, 1997).

### 2.4. fMRI acquisition, design, and analyses

#### 2.4.1. fMRI acquisition

Imaging data for the participants were acquired on a Philips 3 Tesla Achieva TX MR scanner with a 32-channel, phase-array (whole) head coil for all experimental runs. Blood oxygen level-dependent signals were measured with an echo-planar sequence ( $2.5 \times 2.5 \times 3 \text{ mm}$ ; TR 2000ms; TE 35 ms; 35 slices; 250 volumes where the first 2 were discarded to eliminate the effects of start-up transients). For each participant, we additionally acquired a high-resolution ( $1 \text{ mm}^3$ ) anatomical (MPRAGE) scan.

#### 2.4.2. fMRI design and procedures

fMRI runs were arranged in a block-design with each stimulus block lasting 24 secs, and each fixation block lasting 16 secs. One particular scan run included seven main block types comprising six stimulus condition blocks (i.e., low, medium, and high x intact/scrambled) and a fixation block. Each stimulus condition block was repeated twice within a particular run, and was interleaved by a fixation block. Block order was pseudo-randomized such that the intact block was always followed by the corresponding yoked-scrambled condition block, and interleaved by a fixation block (Fig.1b). Individual condition blocks consisted of 6 stimulus presentations comprising 5 unique images selected from the condition-specified set of 15. Within the block, one randomly-selected image was immediately repeated. The subject was asked to perform a *one-back* task, indicating their detection of a repeated image via an MR-compatible button box. Each stimulus was presented for 3 s and was followed by a uniform black screen lasting 1 s during which subjects could respond. During fixation blocks, we presented a static square that was  $6 \text{ deg} \times 6 \text{ deg}$  in size and contained an 'X' in the center. This image was presented identically to the two eyes (i.e., without disparity) in order to promote continued vergence.

We generated three Run variations that differed with respect to the 5 stimulus exemplars that were selected within each condition (e.g., 0-2.5%). This ensured that any repetition effects could be minimized. Run order was counterbalanced both within and across participants, and participants completed a total of 6-8 runs. Each run lasted 8.2 minutes, and participants were encouraged to take breaks in between. Completion of the full session took approximately 80 minutes.

#### 2.4.3. fMRI data analysis

fMRI data were analyzed with BrainVoyager QX (BrainInnovation B.V.). Anatomical data of each observer were used for cortex reconstruction, inflation, and flattening. For each functional EPI, the initial two volumes were discarded in order to eliminate startup transients in the data. Functional data were subsequently pre-processed using three-dimensional motion correction, slice-time correction (with cubic-spline interpolation), spatial smoothing (Gaussian filter, full-width at half maximum, 5 mm; for GLM only), linear trend removal, and highpass filtering (three cycles per run cut-off). The functional images were then aligned to each participant's anatomical data and transformed into Talairach space. All volumes of each observer were aligned to the first functional volume of the first run of the session.

Data were subsequently analyzed both in terms of their univariate activity (GLM), and multivariate patterns (multivoxel pattern analysis, MVPA). GLM analyses included regressors for each experimental condition, and six motion regressors (three translation parameters, in millimeters; and three rotation parameters, pitch, roll, yaw; in degrees) defined as square-wave regressors for each stimulus presentation block convolved with a gamma function to approximate the idealized haemodynamic response. The time course signal of each voxel was then modelled as a linear combination of the different regressors (least-squares

fits) and the regressor coefficients were used for contrasts of the different experimental conditions. We contrasted each main stimulus condition (low, medium, high), with its scrambled-yoked condition (i.e., low-scrambled, medium-scrambled, high-scrambled). As our stimulus setup can be conceptualized as a 3 (density) x 2 (intact/scrambled) design, we also tested for voxels that survive an interaction analysis, changing not only with stimulus coherency, but also with density. Whole-brain, group-level responses were analysed using GLM random-effects analyses.

For the multivariate classifications, we chose to use a linear SVM classifier (libSVM) (Chang, 2011) together with a multivariate feature selection algorithm, Recursive Feature Elimination (RFE) to estimate spatial patterns (De Martino et al., 2008). Using the RFE allowed us to avoid having to select a somewhat arbitrary fixed number of voxels per ROI (as is required in conventional MVPA), and instead offers estimates based on voxel subsets with the best performance within each ROI. Briefly, time-course data at each voxel were first converted into Z scores and shifted in time (4 s). This shift corresponds to the typical peak of the BOLD response function (Serences, 2004). We then took 80% of the training data set to compute SVM weights. Note that the sampling of data for training was done while retaining blocks in their entirety (i.e., no blocks were partitioned). The selection of the data set (and computation of SVM weights) were repeated 20 times within a particular RFE step (i.e., each voxel had 20 sampled weights, which were subsequently averaged). Following each step, we then ordered voxels based on their (step-averaged) weight from the highest to the lowest. Using these weights, we omitted the 5 most uninformative voxels, and used the rest to decode the test patterns. This yielded an accuracy at the current voxel count/pattern. This process was repeated until voxel count fell below 50. For each ROI, based on the maximum mean accuracy (across all cross-validations) across all RFE steps, we retrieved the final voxel pattern with which to compare the accuracies of the different cross validations. Mean prediction accuracies were tested against baseline (0.53) using Bonferroni-corrected t-tests. Baseline was determined via permutation tests for the data (i.e., by running 1,000 SVMs with shuffled labels).

We identified regions of interest (ROIs) and subsequently extracted the individual condition beta-weights and multivariate patterns by first splitting the data of every subject into two sets: an initial set comprising the first run of every subject, and a second set comprising all remaining runs. ROIs were defined as spherical ROIs (5 mm radius) centered on the center of mass of the significant clusters ( $qFDR < .05$ ), as identified from a random effects GLM using the initial set of data. Subsequent analyses were computed by using the second, independent set of data. This ensured that effects that emerge are robust and unhindered by the circularity problem in MR analysis (Kriegeskorte et al., 2010a).

Finally, in order to explore the influences that the identified key regions of interest exert on other regions of the brain, we conducted an effective connectivity analysis adopting the Granger Causality Mapping (GCM) approach (Goebel et al., 2003; Roebroeck et al., 2005). The GCM measures directed influences between brain areas using autoregressive modeling of the fMRI data over time and is particularly useful under contexts for which a pre-specification of models is not intuitive. In short, the GCM quantifies the predictive value of responses in one region (i.e., the seed) for forecasting responses over other regions (here, every voxel) of the brain, pairing the time-course of the seed region with time-course of the voxel and computing influence from the seed to the voxel or vice versa. GCM was conducted within BrainVoyager QX, for each subject, seeding each ROI of interest in turn, for each main condition of interest (low, medium, high densities).

## 2.5. Behavioural tasks (in-laboratory)

Participants were asked to return within two weeks following the MR session in order to complete a set of behavioural tasks. For the behavioural tests, we elected to present distinct density levels across test

runs as we sought to examine any changes in stress ratings that might occur over repeated presentations. This is in contrast to the MR paradigm where we varied density levels within the test run.

### 2.5.1. Visual Analogue Scale (VAS) ratings

The VAS is a widely used tool for rating perceived stress. Here, we adopt the modified protocol introduced by von Dawans (von Dawans et al., 2011) that has been implemented previously in assessments of stress recovery responses due to exposure to images with green-cover (Jiang et al., 2016, 2015). We further adapted the protocol for computer-based use.

Participants completed four stimulus runs, each comprising distinct stimuli (0–2.5%, 10–20%, 31–40%, 61–70%). Each run consisted of three blocks of stimulus presentations lasting 120 secs each (15 stimuli x 8 secs). Participants were asked to complete VAS ratings at the commencement of each stimulus run ( $t_0$ ), and after each block ( $t_1$ ,  $t_2$ ,  $t_3$ ). Completion of the VAS ratings entailed asking subjects to rate their level of each of ‘anxiety’, ‘tension’, and ‘avoidance’, in turn, by adjusting a toggle along a continuous scale, presented on the screen in the form of horizontal line (leftmost indexed 0, reflecting feeling no anxiety/tension/avoidance, and rightmost indexed 1 reflecting feeling maximally anxious/tense/avoidance; selection was not ordinal). For each scale, participants were given a maximum of 10 secs to respond, and were instructed to press a key (space) once satisfied with their selection. Blocks were separated by a 120 sec blank interval during which no stimuli were presented. Run order (i.e., density condition) was randomized within each subject, and each run was separated by a fixed break lasting 300 secs during which no images were presented on the screen. Completion of the full task took approximately 80 minutes.

### 2.5.2. Preference ratings

In this task, participants were presented with 60 stimuli (15 stimuli per density condition – 0–2.5%, 10–20%, 31–40%, 61–70%) in random order. Each stimulus was presented for 8 seconds, after which it was replaced with a blank (mid-grey) screen. For each image, participants were asked to rate on five-point Likert scale, how much they would prefer to ‘take a walk’ in the environment depicted. This paradigm is adapted from that previously used by Jiang et al. (Jiang et al., 2015), the responses for which have been shown to be related to percentage green-cover in the image. For each image, participants were given a maximum of 10 secs to respond and were instructed to press one of five keys (numbered 1–5) to respond. Completion of this task took approximately 10 minutes.

### 2.5.3. Behavioural data analysis

Behavioural performance for the VAS scales was quantified in terms of the mean ratings at each of  $t_1$ ,  $t_2$ , and  $t_3$  normalized to  $t_0$  [ $(t_x - t_0)/(t_x + t_0)$ ]. Performance for the preference rating task was computed as the simple mean rating for each density condition. As response input on both tasks was not permitted until after stimulus offset, reaction time data were not considered informative and not analysed. The data were analyzed with a repeated-measures analysis of variance (ANOVA) comparing ratings across densities (and time points, for the VAS task). All data (except for the Likert rating data of the preference rating task) satisfied parametric assumptions, and any variance (sphericity) violations were addressed with Greenhouse-Geisser corrections. Follow-up post-hoc comparisons were conducted by means of Bonferroni-corrected t tests (two-tailed). Correlations comparing behavioural data versus fMRI (SVM accuracies) were achieved by means of Pearson’s (VAS) or Spearman’s (preference) regressions, corrected to hold family-wise error rate at .05.

## 2.6. Data availability

### 2.6.1. Data availability

The data that support the findings of this study are available at the XNAT public repository [central.xnat.org, project ID: Nature]. All MR

headers were anonymized and T1 images were defaced by means of skull-stripping.

### 2.6.2. Code availability

Custom code written for the presentation of stimuli and/or analyses of data in this manuscript are available from the corresponding authors upon reasonable request.

## 3. Results

### 3.1. Behavioural ratings

We firstly present results from the in-laboratory VAS and preference ratings tests to validate that the static images employed here are effective in inducing variable changes in both stress-related and preference-related mechanisms. Behavioural responses, quantified in terms of mean ratings for each of the VAS categories (avoidance, anxiety, and tension), and for the preference task, were computed for each density condition and are presented in Fig. 1c, d. For the VAS task, ratings at each timepoint ( $t_1$ ,  $t_2$ , and  $t_3$ ) were normalized to ratings obtained at baseline ( $t_0$ ) such that ratings at timepoint  $x$  were normalized in the manner  $[(t_x - t_0)/(t_x + t_0)]$ . Indices were subsequently concatenated across timepoints and tested against zero by means of Bonferroni-corrected t-tests. We found that *avoidance* ratings decreased significantly from baseline at the medium and highest densities [ $t(40) = -2.58$ ,  $p < .01$ ,  $d = .38$  for medium;  $t(40) = -2.89$ ,  $p = .003$ ,  $d = 0.46$  for high]. Further *anxiety* ratings were significantly lower than baseline for the highest density only [ $t(40) = -3.99$ ,  $p < .001$ ,  $d = .65$ ]. *Tension* ratings did not differ from baseline for all densities.

Normalized indices for the VAS task were also tested across timepoints by means of a 4 (density)  $\times$  3 (rating scale)  $\times$  3 (timepoint) repeated-measures ANOVA. The analysis indicated significant main effects of density [ $F(3,90) = 4.1$ ,  $p = .009$ ,  $\eta^2_p = .12$ ] and scale [ $F(2,60) = 6.2$ ,  $p = .004$ ,  $\eta^2_p = .17$ ]. Follow-up comparisons revealed that overall ratings were significantly lower for the highest (61-70%) density as compared to the lowest (0-2.5%) density. The main effect of scale was not further pursued as we did not deem comparisons of ratings among scales to be informative.

Lastly, we computed a one-way repeated-measures ANOVA comparing *preference* ratings across densities (Fig. 1d). We found that preference ratings increased up to the medium density level beyond which they asymptote [ $F(1.3, 50.0) = 10.23$ ,  $p = .001$ ; all pairwise  $ps < .05$  except for medium vs high,  $t(40) = .52$ ,  $p = 1.0$ ]. These results suggest that the static images were indeed effective in eliciting significant changes in stress-related and preference-responses.

### 3.2. fMRI: univariate responses

For the fMRI data, we began by examining univariate (amplitude) responses. To do so, we took firstly a subset of the data (1 run per subject) and performed a whole-brain contrast using a general linear model (GLM), comparing responses of *all* intact green-space images (low, medium, high, collapsed) versus responses for their yoked-scrambled conditions (collapsed). We found significant clusters ( $qFDR < .05$ ) in bilateral posterior cingulate (dorsal dPCC, ventral vPCC), superior temporal gyrus (STG), superior parietal lobule (SPL), middle frontal gyrus (mFG), precentral gyrus (PCG), visual cortex/cuneus (Cu), and the medial dorsal nucleus of the thalamus (MD) (Fig. 2a; Supplementary Table S1).

In order to better quantify the univariate responses in these regions, we then extracted beta weights from spherical ROIs (5 mm rad.) centered on these clusters using the remaining data from each subject (Fig. 2b). Note that splitting the data for the identification of ROIs on the one hand, and all subsequent analyses, on the other, ensured that effects that emerge are robust and unhindered by the circularity problem in MR analysis (Kriegeskorte et al., 2010b). For greater clarity, in Fig. 2b, we

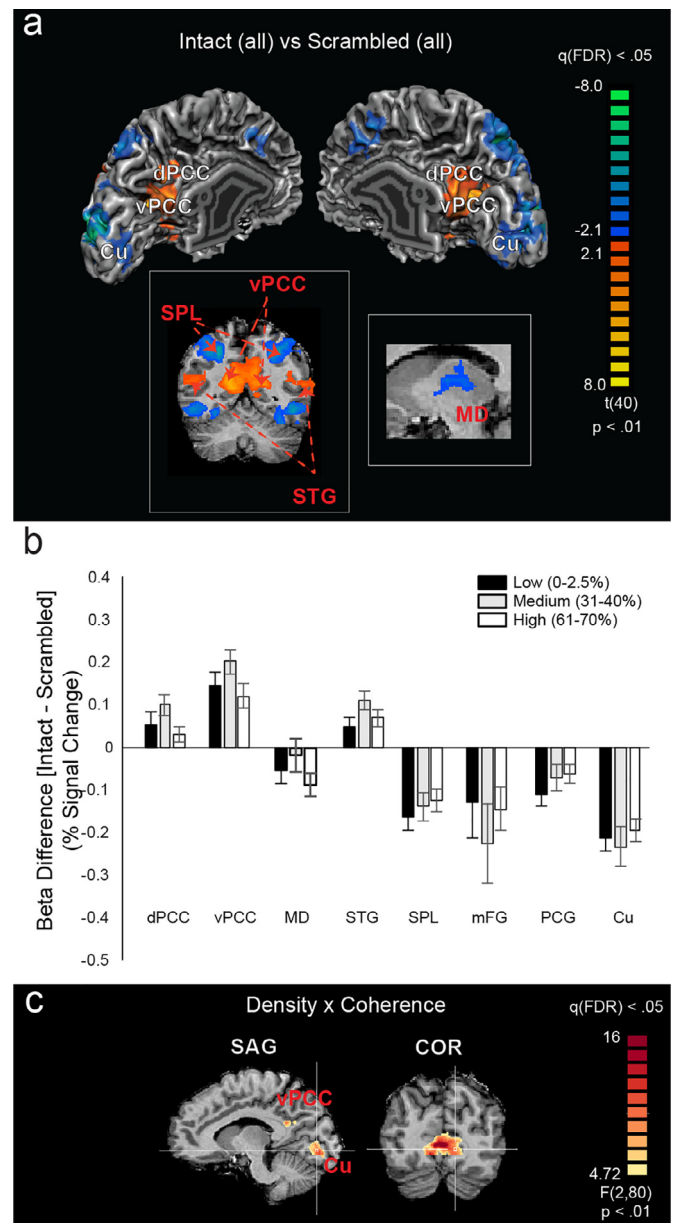


**Fig. 2.** (a) Results from a group-level GLM contrast between all intact density conditions versus all scrambled conditions. Responses are superimposed onto representative surface meshes of one participant. Sulci are coded in darker grey than the gyri. In the insets, better visualizations of the SPL, STG, dPCC, vPCC, and the MD are provided. (b) Differences in GLM beta weights (intact - scrambled) for the three main green-space densities. Error bars represent  $\pm 1$  standard error of the mean. (c) Results from the whole-brain interaction (density  $\times$  coherence) analysis, overlaid on a Talairach-transformed brain. (For interpretation of the references to color in the text, the reader is referred to the web version of this article.)

present indexed responses for each ROI, computed as the difference in beta weights between each condition and its corresponding scrambled condition. Raw (un-indexed) weights were entered into a 2 (coherence: intact/scrambled)  $\times$  3 (density)  $\times$  8 (ROI) repeated-measures ANOVA. The analysis indicated that responses in the (dorsal and ventral) PCC and STG were significantly higher for intact versus scrambled images [coherence  $\times$  ROI interaction,  $F(1.96, 78.5) = 32.7$ ,  $p < .001$ ,  $\eta^2_p = .45$ ; t-test (coherence) for dPCC,  $t(40) = 5.1$ ,  $p < .001$ ;  $t(40) = 8.4$ ,  $p < .001$  for vPCC;  $t(40) = 7.3$ ,  $p < .001$  for STG]. By contrast, responses in SPL, mFG, and the Cuneus were significantly higher for the scrambled ver-

sus intact images [t-test (coherence) for SPL,  $t(40) = -7.4$ ,  $p < .001$ ;  $t(40) = -3.3$ ,  $p = .002$  for mFG;  $t(40) = -10.5$ ,  $p < .001$  for Cuneus]. Univariate responses in all ROIs did not differ significantly across densities [main effect of density,  $F(2,80) = .049$ ,  $p = .95$ ,  $\eta^2_p = .001$ ; no interaction involving density].

Finally, we entered all data into a whole-brain (Random Effects) GLM analysis that probed the interaction between density (low, medium, high) and coherence (intact/scrambled). The analysis revealed two clusters ( $qFDR < .05$ ) located at the vPCC ([Tal  $+/-9$ ,  $-47$ ,  $21$ ]) and Cuneus ([Tal  $+/-9$ ,  $-75$ ,  $-5$ ]) (Fig. 2c). Our identification of these clusters to be differentially responsive to green-space density above and beyond lower order differences (i.e., coherency), aligns, at least qualitatively, with the univariate trends observed from the ROI-analysis (c.f., Fig. 2b), showing for the vPCC, the greatest response difference (intact – scrambled) at the medium density, and for the Cuneus, the greatest response difference (scrambled – intact) at again, the medium density. The three-way interaction in the ROI analysis did not survive statistical correction, however.

### 3.3. fMRI: patterned-responses

Examination of pattern-level responses was more revealing. We performed a support vector machine (SVM)-based multivariate pattern analysis (MVPA) by extracting firstly, for each ROI and each condition, beta values. These beta values were then contrasted, (i.e., Low Intact - Low Scrambled), yielding voxel-wise patterns now representing beta-contrasts. We then performed classifications for the resulting ‘beta contrast patterns’, comparing for each ROI, all possible combinations of the three green-space densities [e.g., (Low Intact - Low Scrambled) vs (Medium Intact - Medium Scrambled)]. The classification accuracies of all ROIs are presented in Fig. 3a. SVM accuracies were firstly tested against a baseline of 0.52, as obtained via permutation tests with shuffled condition labels, by means of Bonferroni-corrected t-tests (see Methods).

The analyses revealed above-baseline discrimination performance in vPCC [(Low Intact - Low Scrambled) vs (Medium Intact - Medium Scrambled);  $t(40) = 2.53$ ,  $p = .007$ ; (Low Intact - Low Scrambled) vs (High Intact - High Scrambled);  $t(40) = 4.19$ ,  $p < .001$ ] and the Cuneus [(Low Intact - Low Scrambled) vs (Medium Intact - Medium Scrambled);  $t(40) = 3.72$ ,  $p < .001$ ; (Low Intact - Low Scrambled) vs (High Intact - High Scrambled);  $t(40) = 5.61$ ,  $p < .001$ ] only.

SVM accuracies were additionally entered into a 3 (density) x 8 (ROI) repeated-measures ANOVA. The analysis indicated a significant main effect of ROI,  $F(7, 280) = 11.2$ ,  $p < .001$ ,  $\eta^2_p = .219$ , and a significant density x ROI interaction [ $F(14, 560) = 1.85$ ,  $p = .04$ ,  $\eta^2_p = .044$ ]. The interaction was followed-up by separate one-way ANOVAs comparing accuracies for the three density comparisons within each ROI. The analyses indicated that accuracies among the three comparisons varied significantly for the vPCC and Cuneus only [ $F(2,80) = 5.2$ ,  $p = .008$ ,  $\eta^2_p = .114$  for vPCC;  $F(2,80) = 4.38$ ,  $p = .016$ ,  $\eta^2_p = .10$  for Cuneus]. In both ROIs, accuracies for the middle comparison [(Low Intact - Low Scrambled) vs (High Intact - High Scrambled)] were significantly higher than accuracies for the [(Medium Intact - Medium Scrambled) vs (High Intact - High Scrambled)] comparison [ $t(40) = 3.4$ ,  $p = .005$  for vPCC;  $t(40) = 2.92$ ,  $p = .018$  for Cuneus].

### 3.4. Brain-behaviour correlations

In order to further establish the roles of the vPCC and Cuneus, we correlated individual subject SVM accuracies with behavioural VAS and preference ratings using data collapsed across time-points. We elected to use the SVM data from the [(Low Intact - Low Scrambled) - (High Intact - High Scrambled)] comparison as it yielded the highest SVM accuracies among all comparisons. These SVM accuracies were correlated with a behavioural index computed, for each scale, by subtracting

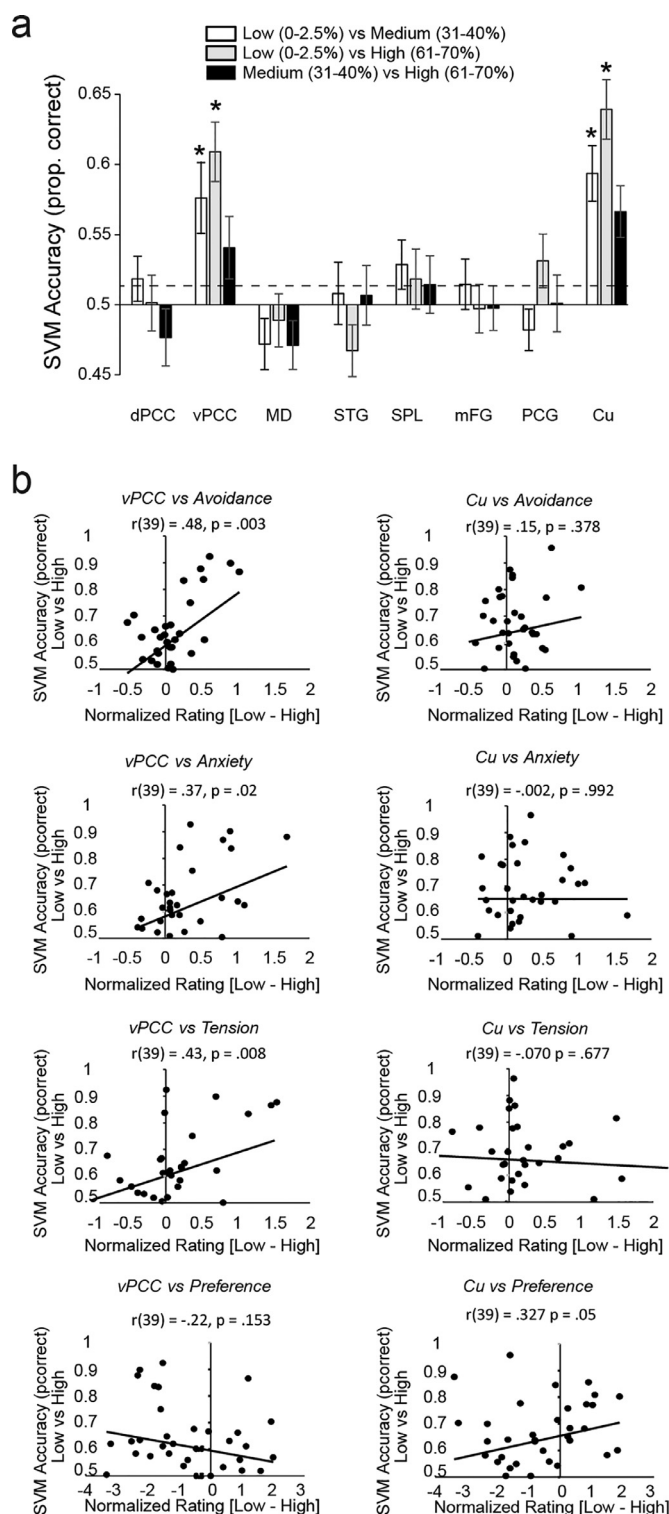


Fig. 3. (a) SVM accuracies for discriminating beta contrast patterns among differing density conditions, e.g., [(Low Intact vs Low Scrambled) vs (Medium Intact vs Medium Scrambled)]. Asterisks denote above-baseline (0.52, dashed line) accuracies. Error bars represent  $\pm 1$  standard error of the mean. (b) Correlations between VAS and preference ratings, and SVM accuracies.

behavioural ratings for the highest density (61–70%) condition from those for the lowest (0–2.5%) density condition. We found a significant correlation between SVM accuracies of the vPCC with avoidance ratings [ $r(39) = .48, p = .003$ ], such that individuals with higher pattern-discriminability for the low vs high beta contrast patterns in the vPCC also tended to report larger reductions in avoidance (Fig. 3b). Ratings for anxiety, and in particular tension trended towards a similar correlation with the behavioural index, but did not survive an 8-way statistical correction [vPCC vs. anxiety,  $r(39) = .37, p = .02$ ; vPCC vs. tension,  $r(39) = .43, p = .008$ ]. Further, preference ratings also did not significantly predict SVM accuracies [vPCC vs. preference,  $r(39) = .22, p = .17$ ]. Finally, SVM accuracies for the Cuneus did not correlate with VAS nor preference ratings.

As behavioural metrics were acquired systematically over three time-points within the testing session,  $t_1$ ,  $t_2$ , and  $t_3$ , we proceeded to test for correlations at each of these timepoints (Supplementary Table S2). We observed significant correlations implicating all three rating scales at all time points – though only several survive a 9-way statistical correction: Tension at  $t_1$ ,  $r(39) = .49, p = .002$ ; Anxiety at  $t_2$ ,  $r(39) = .45, p = .004$ , and Avoidance at  $t_3$ ,  $r(39) = .46, p = .003$ .

Finally, we probed correlations using GLM responses in place of SVM accuracies. In order to approximate these comparisons to those performed using the SVM data, we entered GLM responses from the conjunctive comparison [(Low Intact – Low Scrambled) – (High Intact – High Scrambled)]. We observed no correlations among all comparisons (Supplementary Table S3).

### 3.5. In-bore performance (one-back task)

We examined performance on the one-back task performed in-bore, by computing detection sensitivities ( $d'$ ) across densities, for each subject. Sensitivity indices were entered into a 2 (coherence: intact/scrambled)  $\times$  3 (density) ANOVA that indicated a significant main effect of coherence [ $F(1,40) = 18.6, p < .001, \eta^2_p = .32$ ], such that sensitivity was lower for the scrambled versus intact images. Performance did not differ across densities [ $F(2,80) = 1.35, p = .27, \eta^2_p = .033$ ] (Supplementary Fig. S1).

### 3.6. Hemispheric comparisons

We conducted further analyses examining GLM responses and SVM classification performance separately for the left and right hemispheres across all cortical ROIs. The results are presented in Supplementary Fig. S2. GLM beta weights were entered in to a 2 (hemisphere)  $\times$  2 (coherence: intact/scrambled)  $\times$  3 (density)  $\times$  8 (ROI) ANOVA that indicated no significant main effect of hemisphere [ $F(1,40) = .778, p = .38, \eta^2_p = .019$ ], nor any interactions involving hemisphere. Similarly, SVM accuracies for discriminating between beta contrast patterns among the three densities were entered in to a 2 (hemisphere)  $\times$  3 (density)  $\times$  8 (ROI) ANOVA that indicated no significant main effect of hemisphere [ $F(1,40) = .723, p = .400, \eta^2_p = .018$ ], nor any interactions involving hemisphere.

### 3.7. Effective connectivity

Finally, we sought to test the effective connectivity (i.e., directional interactions) among the key regions of the brain implicated during the viewing of green urban landscapes. Results from the GCM analysis are presented in Fig. 4. Here, directed GCM values (dGCM) reflect the difference of seed-to-voxel minus voxel-to-seed influences. Hence, a positive dGCM value indicates a greater feedforward versus feedback influence, and a negative dGCM value indicates a greater feedback versus feedforward influence. dGCM map values for all subjects were tested against zero. For brevity, we present a sample group-level map ( $p < .0167$ ) seeding the vPCC, during the viewing of landscapes with high-density green-

space (i.e., high density, intact condition) in Fig. 4a. As can be seen in this Fig., activity in vPCC is predictive of activity in much of the same regions identified from our initial univariate contrast (all intact vs all scrambled). To better quantify the directed influence of each of the key ROIs (vPCC, Cu, selected as patterned-responses of these regions varied with changes in green-space density) on the remaining ROIs, we proceeded to extract for each seed, dGCM values for the remaining ROIs, and for each of the low, medium, and high density conditions (Fig. 4b). dGCM values for each ROI were tested against zero (Bonferroni-24-way-corrected t-tests, two-tailed; non-zero ROIs denoted by asterisks). These analyses revealed that the vPCC exerts dominantly feedforward influence on the spatial and attentional regions (dPCC, SPL, mFG), as well as the cuneus. By contrast, activity of the cuneus exerts greater feedforward influences on the dPCC, STG, SPL, and mFG but for the high density condition only.

As for this last analysis, we entered data from the intact conditions only, a concern remains that we are unable to tease out the extent to which these connectivity metrics reflect the responses to lower order features. To mitigate this problem, we replicated the GCM analyses, entering instead data for all the scrambled conditions. Any connectivity influences observed previously using the intact images that relate to lower-order features only would also be picked up by this analysis. In Fig. 4c, we plot  $\Delta$  GCM values, obtained by subtracting the GCM data of the scrambled condition from those of the intact condition. Positive values here reflect greater feedforward influence from the intact versus scrambled seeds. Both sets of data (obtained using the intact and scrambled conditions as seeds) were entered in a grand 2 (seed ROI)  $\times$  3 (density)  $\times$  8 (target ROI)  $\times$  2 (coherence) ANOVA that indicated a significant main effect of density [ $F(2,78) = 3.34, p = .04, \eta^2_p = .079$ ]. There were also significant main effects of coherence [ $F(1, 40) = 6.3, p = .016, \eta^2_p = .136$ ], ROI [ $F(7,280) = 10.63, p < .001, \eta^2_p = .21$ ], a three-way seed  $\times$  coherence  $\times$  ROI interaction [ $F(7, 280) = 7.00, p < .001, \eta^2_p = .149$ ], and a three-way seed  $\times$  density  $\times$  ROI interaction [ $F(14,560) = 8.9, p < .001, \eta^2_p = .182$ ].

The seed  $\times$  coherence  $\times$  ROI interaction was followed up by separate two-way ANOVAs for the two seeds. The analysis for the vPCC indicated that feedforward influences towards the SPL were significantly greater for the intact than scrambled conditions [coherence  $\times$  ROI interaction,  $F(7, 280) = 22.67, p < .001, \eta^2_p = .362$ ; SPL,  $t(40) = 6.24, p < .001$ ]. By contrast, the analysis for the Cuneus indicated that influences towards all ROIs did not significantly differ between intact and scrambled conditions.

Finally, the seed  $\times$  density  $\times$  ROI interaction was further probed by separate density  $\times$  ROI ANOVAs for the two seeds. The analysis for the vPCC indicated that its feedforward influence towards all ROIs decreased systematically with increases in density [ $F(2,80) = 3.9, p = .024, \eta^2_p = .089$ ], although the magnitude of the feedforward influence was greater towards the dPCC, SPL, MFG and Cuneus, than towards all remaining ROIs [ $F(7,280) = 10.6, p < .001, \eta^2_p = .21$ ]. By contrast, the analysis for the Cuneus indicated that its influences towards all ROIs did not differ across the three densities [ $F(2,80) = 2.54, p = .086, \eta^2_p = .06$ ], although their magnitudes and directionalities differed across the ROIs [ $F(7,280) = 24.85, p < .001, \eta^2_p = .38$ ]. In particular, the Cuneus exerts feedforward influence on dPCC, MD, STG, SPL and MFG, while receiving feedback influence from vPCC and PCG.

Taken together, the dGCM results suggest that green-space scenes drive a shift in effective connectivity such that during the viewing of these scenes, the vPCC exerts significant feedforward influence towards visuo-attentional regions, including in particular the SPL, the influence towards which reflects more than modulations driven by lower-order features. Directed influences from the vPCC notably declines systematically with increases with green-space density. By contrast, while the Cuneus exerts feedforward influence to a number of the same visuo-attentional regions, it also receives significant feedback influence from the vPCC and PCG. Critically, directed influences from the Cuneus do not differ across the three densities.

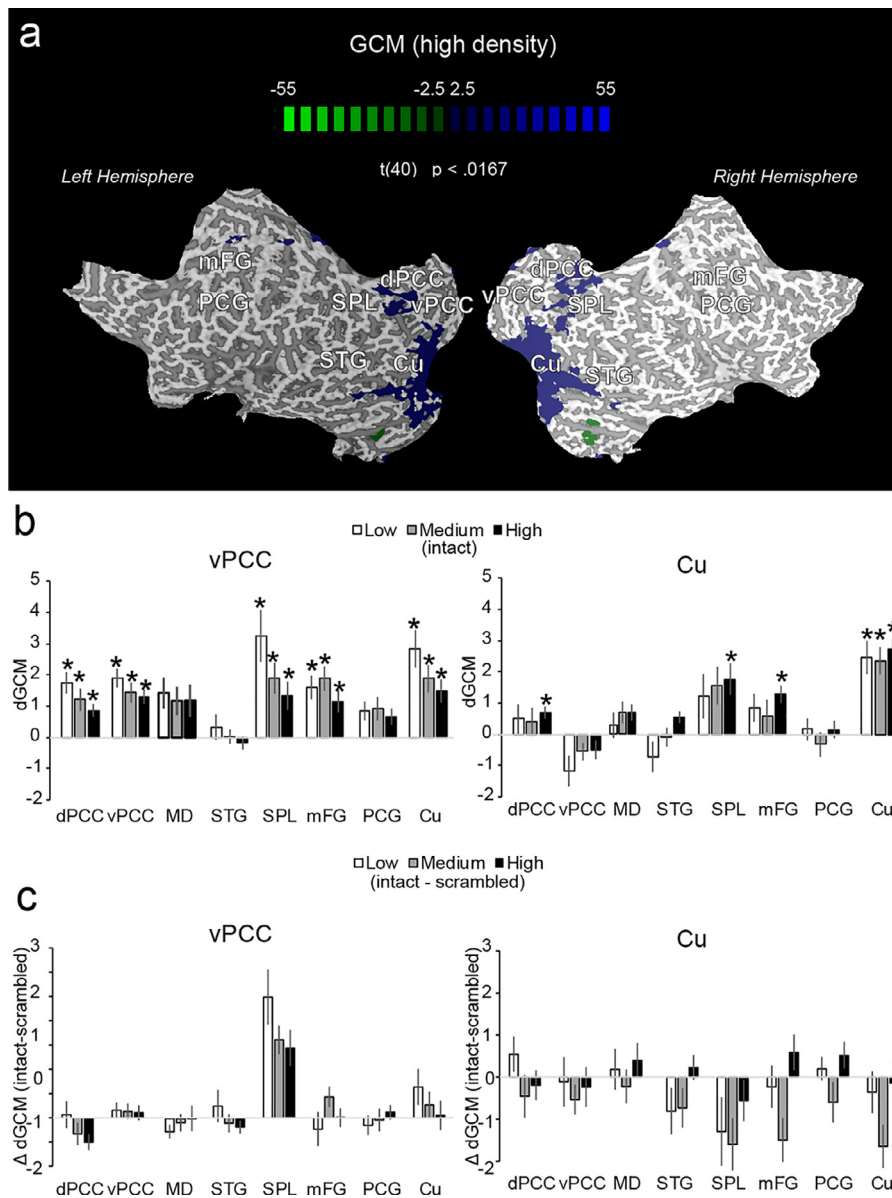


**Fig. 4.** Results from the Granger Causality Mapping analysis. (a) Sample whole-brain map seeding the vPCC for the high green-space density presentations. dGCM maps from all subjects were tested against a value of zero ( $p < .0167$ ). As the dGCM reflects a difference between seed-to-voxel minus voxel-to-seed, positive (blue) values denote dominant feedforward influences, and negative (green) values denote dominant feedback influences. (b) Mean dGCM values extracted following the seeding of the vPCC and Cu (intact images). Asterisks denote ROIs with mean dGCM values that are significantly different from zero following a 24-way statistical correction. (c) Mean difference in dGCM values obtained by subtracting dGCM scrambled from dGCM intact. Error bars represent  $\pm 1$  standard error of the mean. (For interpretation of the references to color in the text, the reader is referred to the web version of this article.)

#### 4. Discussion

Our data indicate that green urban landscapes elicit substantial activity along a network of regions that have been commonly implicated for spatial processing (SPL, STG), spatial and executive attention (PCC, SPL, mFG), and sensory encoding (Cu). While activity of the cuneus most likely reflects irrelevant lower-order (visual) differences between the coherent versus scrambled images, the implication of attention-related regions, including the mFG – constituting part of the prefrontal cortex – is also not all that surprising in light of previous work that has reported these regions to be responsive during the perception of natural (e.g., mountain, forest, water) versus artificial (urban) environments (Tang et al., 2017), or to be affected by short periods of walks through natural versus urban settings (Bratman et al., 2015). Our data suggest that modulations of responses in these same regions can be observed within urban contexts alone, with transient presentations of urban landscapes that vary parametrically in terms of their *naturalness* (i.e., green-space density). The involvement of attention-related regions during the perception of natural landscapes has been interpreted with the respect to the capacity of natural images to drive attention restora-

tion (Kaplan, 1995) – the notion that natural environments allow a disengagement of effortful directed attentional mechanisms.

Critically, our data draw out a potentially key role of the (ventral) PCC for moderating stress-related responses to urban landscape images. Responses of this region, along with those of the Cuneus varied with changes in green-space density (after accounting for responses driven by lower-order features). Only responses of the vPCC appear to be functionally relevant to behavioural stress metrics, however. In particular, patterned responses of the vPCC, and in particular density-related changes in these responses, well-match behavioural changes in VAS avoidance ratings. Responses of the vPCC also predicted, to a weaker extent, density-related changes in anxiety and tension ratings though these two correlations did not survive the 8-way statistical correction (Fig. 3b). Notably, our effects cannot be due to variances in attention across conditions as performance on the one-back task performed in bore, quantified in terms of  $d'$  detection sensitivity, was comparable across all density conditions (Supplementary Fig. S1).

The human posterior cingulate has been historically treated as a unitary region that constitutes part of the emotion-regulating limbic system

(Papez, 1937), although it has also been implicated in motivation, reward, and valuation, activating with changes in subjective motivational state (Small et al., 2001). The PCC is regarded as a key node of the default mode network and is now thought to have functionally segregated dorsal and ventral portions that are differentially involved in cognitive control (Leech and Sharp, 2014). The classically defined ventral posterior cingulate (BA23), and in particular the ventral bank of the cingulate gyrus constituting Brodmann areas 29/30 (i.e., the retrosplenial cortex; RSC) towards which our activity extends, has been implicated in spatial memory and navigation (e.g., Czajkowski et al., 2014; Wolbers and Büchel, 2005), topographical estimations (Aguirre and D'Esposito, 1999), including mapping between egocentric and allocentric reference frames for orienting in an environment (Committeri et al., 2004; Epstein, 2008; Kravitz et al., 2011; Vann et al., 2009). The RSC has been shown to respond strongly to familiar (visual) landmarks and locations (Ghaem et al., 1997; Rosenbaum et al., 2004).

We conjecture that green urban landscapes moderate stress-related responses through engaging the vPCC, including the spatially-sensitive RSC, which drives regulatory responses initiated through the prefrontal and hippocampal cortex and ultimately, the neuroendocrine system. How might this be achieved? The vPCC has extensive reciprocal connections with other limbic and paralimbic structures, the temporal cortex (Kobayashi and Amaral, 2007), and the ventromedial prefrontal cortex (Vogt and Pandya, 1987). These connections are absent or are less dense in the dPCC. Interestingly, while the PCC also has extensive bidirectional projections to subcortical centers including the thalamus, it has few (if any) connections to primary sensory and motor cortex (Parvizi et al., 2006), consistent with a role for this region that is well-removed from lower-order sensory and motor functions. If we consider the RSC specifically, this region carries substantial reciprocal connections, particularly from BA30 with the dorsolateral prefrontal cortex (Goldman-Rakic et al., 1984), the parahippocampal cortex, and the entorhinal cortex (Suzuki and Amaral, 1994), although it also projects to the superior temporal and posterior parietal cortex (Morris et al., 1999). Notably, through in particular its connections with the PFC and hippocampus, regions that also carry their own projections towards the hypothalamic (paraventricular) region (Buijs and Van Eden, 2000), the RSC and the vPCC at large are well equipped to interface with the neuroendocrine system.

Results from our effective connectivity (Granger Causality Mapping) analysis appear to be congruent with the idea that if indeed the (ventral) cingulate cortex plays a key role in stress-regulation, it is engaged early during the viewing of green urban landscapes. We observed predominantly feedforward influences of activity from this region to the body of spatial and attentional-related regions of cortex. Curiously, feedforward influences exerted by the vPCC decline with the presentation of landscapes with increasing greens-space density. A parsimonious explanation is that landscapes with a lower degree of green-cover may require more active attentional engagement and maintenance mechanisms relative to images with higher levels of green-cover – an explanation that would also be congruent with current attention-restoration theories for the benefits of nature exposure (Kaplan, 1995).

Validating the role of the PCC in particular as it relates to stress-regulatory mechanisms and more broadly, mental health, is of particular clinical importance as this structure shows abnormalities in diseases (Alzheimer's) (Minoshima et al., 1997), neuropsychological disorders (schizophrenia, depression, autism, attention deficit hyperactivity disorder) (Harrison et al., 2007; Ho et al., 1996; Nakao et al., 2011; Pierce et al., 2004; Pol et al., 2001), and in ageing (Andrews-Hanna et al., 2007). The PCC also shows abnormal function following traumatic brain injury (Bonnelle et al., 2011). Our findings that green urban landscapes can elicit systematic changes in responses in this region that are paralleled by changes in stress-ratings, then, raise an intriguing therapeutic potential for natural environmental exposure.

Consistent with data reported by Jiang et al. (Jiang et al., 2016, 2015), it is somewhat curious that changes in preference responses do

not match those for stress-related measures, with the former reaching asymptote by the mid-range green-space density, and the latter continuing to decline with further increases in green-space towards the highest density. These data, considered together with the (lack of) correspondence between preference ratings and fMRI responses suggest that general environmental preference may be driven by activity across a network of regions rather than any singular node identified here. By contrast, urban green content appears to have a more immediate effect on the stress-regulatory system via the posterior cingulate. Still, the exact relevance of the vPCC towards green-space-driven stress-regulation awaits further clarification. In particular, we found here that green-spaces elicited strong behavioural reductions of stress, but for the avoidance (and to a lesser extent, anxiety) sub-metrics only. We speculate that our inability to find tension-related effects (extending to the correspondingly weak brain-behaviour correspondences) may be due to low levels of baseline tension in the laboratory setting (5%), relative to the other two metrics (10-20%). Further empirical work will be required to better establish the potency of green-space exposure in relation to these metrics, perhaps through the inclusion of psychological stressors.

We used systematic manipulations of natural content to elicit corresponding changes in the brain in order to probe the circuitry that gives natural environments the capacity to drive health benefits. We started here by manipulating an obvious feature of natural environments – green cover – while holding constant the environmental context (i.e., urban residential setting) and reducing differences in other potentially irrelevant sensorial features.

Our data beg further investigations as to what other features of natural environments, beyond green-space density may be modifiable elements that can be utilized by city-planners and health practitioners alike to promote brain and mental health. We now know, for example, that natural scenes contain characteristic distributions of luminance and chrominance (Field, 1987; Thomson, 1999; Van der Schaaf and van Hateren, 1996), as well as characteristic second order structure that defines features such as edges and lines (Thomson et al., 2000). Deviations of these dimensions from scale-invariant naturalistic profiles are enough to elicit visual discomfort, headaches, and even seizures in photosensitive individuals (Chatrian et al., 1970; Wilkins et al., 1975). Indeed, image features have been shown to predict the perception of naturalness and aesthetic judgments of natural and man-made scenes (Berman et al., 2014; Ibarra et al., 2017; Kardan et al., 2015). In this vein, it would be interesting to ask whether stress-responses deviate systematically with deviations of the sensory information from their natural profiles – information that could be key to urban design and policy-making. Finally, if indeed vPCC plays a key role in moderating nature-driven benefits to mental health, it may be worth probing how its influence changes across the lifespan, particularly in light of work showing that children, in contrast to adults, have stronger preferences for urban over natural environments (Meidenbauer et al., 2019). Understanding the optimal environmental characteristics for eliciting healthy stress-responses would have far-reaching consequences not only towards understanding the neuroscience of healthy systems, but also for rehabilitative, economic and environmental sectors.

## Acknowledgments

This research was supported by research funding from the Faculty of Architecture and Faculty of Social Sciences, The University of Hong Kong, Faculty Startup Funds (Faculty of Architecture) to BJ, and The University of Hong Kong May Endowed Professorship in Neuropsychology to TL. We thank Shutian Xue, Ailene Chan, Lawrence Kwan, and Alice Leung for assistance in behavioural data collection. We also thank William C. Sullivan (University of Illinois at Urbana-Champaign) for sharing the landscape videos from which this study's stimuli were derived.

## Author contributions

TL, CW, DC, and BJ conceptualized the study. BJ provided the stimuli. DC developed and prepared protocols for MR and behavioural testing, and performed data analyses. DC, NW, and JW were involved in MR data acquisition. All authors contributed to the preparation of this manuscript.

## Data/code availability

**Data availability.** The data that support the findings of this study are available at the XNAT public repository [central.xnat.org, project ID: Nature]. All MR headers were anonymized and T1 images were defaced by means of skull-stripping.

**Code availability.** Custom code written for the presentation of stimuli and/or analyses of data in this manuscript are available from the corresponding authors upon reasonable request.

## Declaration of Competing Interests

The authors declare no competing financial interests.

## Supplementary materials

Supplementary material associated with this article can be found, in the online version, at doi:10.1016/j.neuroimage.2020.117555.

## References

- Aguirre, G.K., D'Esposito, M., 1999. Topographical disorientation: a synthesis and taxonomy. *Brain* 122, 1613–1628.
- Alcock, I., White, M.P., Wheeler, B.W., Fleming, L.E., Depledge, M.H., 2014. Longitudinal effects on mental health of moving to greener and less green urban areas. *Environ. Sci. Technol.* 48, 1247–1255.
- Andrews-Hanna, J.R., Snyder, A.Z., Vincent, J.L., Lustig, C., Head, D., Raichle, M.E., Buckner, R.L., 2007. Disruption of large-scale brain systems in advanced aging. *Neuron* 56, 924–935. doi:10.1016/j.neuron.2007.10.038, https://doi.org/.
- Berman, M.G., Hout, M.C., Kardan, O., Hunter, M.R., Yourganov, G., Henderson, J.M., Hanayik, T., Karimi, H., Jonides, J., 2014. The perception of naturalness correlates with low-level visual features of environmental scenes. *PLOS ONE* 9, e114572. doi:10.1371/journal.pone.0114572, https://doi.org/.
- Berman, M.G., Jonides, J., Kaplan, S., 2008. The cognitive benefits of interacting with nature. *Psychol. Sci.* 19, 1207–1212.
- Berman, M.G., Kross, E., Krpan, K.M., Askren, M.K., Burson, A., Deldin, P.J., Kaplan, S., Sherdell, L., Gotlib, I.H., Jonides, J., 2012. Interacting with nature improves cognition and affect for individuals with depression. *J. Affect. Disord.* 140, 300–305.
- Bonnelle, V., Leech, R., Kinnunen, K.M., Ham, T.E., Beckmann, C.F., Boissezon, X.D., Greenwood, R.J., Sharp, D.J., 2011. Default mode network connectivity predicts sustained attention deficits after traumatic brain injury. *J. Neurosci.* 31, 13442–13451. doi:10.1523/JNEUROSCI.1163-11.2011, https://doi.org/.
- Brainard, D.H., 1997. The psychophysics toolbox. *Spat. Vis.* 10, 433–436. doi:10.1163/156856897X00357, https://doi.org/.
- Bratman, G.N., Hamilton, J.P., Hahn, K.S., Daily, G.C., Gross, J.J., 2015. Nature experience reduces rumination and subgenual prefrontal cortex activation. *Proc. Natl. Acad. Sci.* 112, 8567–8572.
- Buijs, R.M., Van Eden, C.G., 2000. The integration of stress by the hypothalamus, amygdala and prefrontal cortex: balance between the autonomic nervous system and the neuroendocrine system. In: *Progress in Brain Research*. Elsevier, pp. 117–132.
- Chang, C.-C., 2011. "LIBSVM: a library for support vector machines. *ACM Trans. Intelligent Syst. Technol.* 2 (27), 1–27 27, 2011. Httpwww Csie Ntu Edu Tw~ Cjlinlibsvm 2.
- Chatrjian, G.E., Lettich, E., Miller, L.H., Green, J.R., 1970. Pattern-sensitive epilepsy. *Epilepsia* 11, 125–149. doi:10.1111/j.1528-1157.1970.tb03876.x, https://doi.org/.
- Committeri, G., Galati, G., Paradis, A.-L., Pizzamiglio, L., Berthoz, A., LeBihan, D., 2004. Reference frames for spatial cognition: different brain areas are involved in viewer-, object-, and landmark-centered judgments about object location. *J. Cogn. Neurosci.* 16, 1517–1535.
- Czajkowski, R., Jayaprakash, B., Wiltgen, B., Rogerson, T., Guzman-Karlsson, M.C., Barth, A.L., Trachtenberg, J.T., Silva, A.J., 2014. Encoding and storage of spatial information in the retrosplenial cortex. *Proc. Natl. Acad. Sci.* 111, 8661–8666.
- De Martino, F., Valente, G., Staeren, N., Ashburner, J., Goebel, R., Formisano, E., 2008. Combining multivariate voxel selection and support vector machines for mapping and classification of fMRI spatial patterns. *Neuroimage* 43, 44–58.
- Epstein, R.A., 2008. Parahippocampal and retrosplenial contributions to human spatial navigation. *Trends Cogn. Sci.* 12, 388–396.
- Field, D.J., 1987. Relations between the statistics of natural images and the response properties of cortical cells. *Josa A* 4, 2379–2394.
- Ghaem, O., Mellet, E., Crivello, F., Tzourio, N., Mazoyer, B., Berthoz, A., Denis, M., 1997. Mental navigation along memorized routes activates the hippocampus, precuneus, and insula. *Neuroreport* 8, 739–744.
- Goebel, R., Roebroeck, A., Kim, D.-S., Formisano, E., 2003. Investigating directed cortical interactions in time-resolved fMRI data using vector autoregressive modeling and Granger causality mapping. *Magn. Reson. Imaging* 21, 1251–1261.
- Goldman-Rakic, P.S., Selemon, L.D., Schwartz, M.L., 1984. Dual pathways connecting the dorsolateral prefrontal cortex with the hippocampal formation and parahippocampal cortex in the rhesus monkey. *Neuroscience* 12, 719–743.
- Harrison, B.J., Yücel, M., Pujol, J., Pantelis, C., 2007. Task-induced deactivation of mid-line cortical regions in schizophrenia assessed with fMRI. *Schizophr. Res.* 91, 82–86. doi:10.1016/j.schres.2006.12.027, https://doi.org/.
- Ho, A.P., Gillin, J.C., Buchsbaum, M.S., Wu, J.C., Abel, L., Bunney, W.E., 1996. Brain glucose metabolism during non-rapid eye movement sleep in major depression: a positron emission tomography study. *Arch. Gen. Psychiatry* 53, 645–652.
- Ibarra, F.F., Kardan, O., Hunter, M.R., Kotabe, H.P., Meyer, F.A., Berman, M.G., 2017. Image feature types and their predictions of aesthetic preference and naturalness. *Front. Psychol.* 8, 632.
- Jiang, B., Larsen, L., Deal, B., Sullivan, W.C., 2015. A dose–response curve describing the relationship between tree cover density and landscape preference. *Landscape Urban Plan.* 139, 16–25.
- Jiang, B., Li, D., Larsen, L., Sullivan, W.C., 2016. A dose-response curve describing the relationship between urban tree cover density and self-reported stress recovery. *Environ. Behav.* 48, 607–629.
- Kaplan, S., 1995. The restorative benefits of nature: toward an integrative framework. *J. Environ. Psychol.* 15, 169–182.
- Kardan, O., Demiralp, E., Hout, M.C., Hunter, M.R., Karimi, H., Hanayik, T., Yourganov, G., Jonides, J., Berman, M.G., 2015. Is the preference of natural versus man-made scenes driven by bottom-up processing of the visual features of nature? *Front. Psychol.* 6. doi:10.3389/fpsyg.2015.00471, https://doi.org/.
- Kobayashi, Y., Amaral, D.G., 2007. Macaque monkey retrosplenial cortex: III. Cortical efferents. *J. Comp. Neurol.* 502 (5), 810–833.
- Kravitz, D.J., Saleem, K.S., Baker, C.I., Mishkin, M., 2011. A new neural framework for visuospatial processing. *Nat. Rev. Neurosci.* 12, 217–230.
- Kriegeskorte, N., Lindquist, M.A., Nichols, T.E., Poldrack, R.A., Vul, E., 2010a. Everything you never wanted to know about circular analysis, but were afraid to ask. *J. Cereb. Blood Flow Metab.* 30, 1551–1557.
- Kriegeskorte, N., Lindquist, M.A., Nichols, T.E., Poldrack, R.A., Vul, E., 2010b. Everything you never wanted to know about circular analysis, but were afraid to ask. *J. Cereb. Blood Flow Metab.* 30, 1551–1557.
- Leech, R., Sharp, D.J., 2014. The role of the posterior cingulate cortex in cognition and disease. *Brain* 137, 12–32. doi:10.1093/brain/awt162, https://doi.org/.
- Meidenbauer, K.L., Stenfors, C.U.D., Young, J., Layden, E.A., Schertz, K.E., Kardan, O., Decety, J., Berman, M.G., 2019. The gradual development of the preference for natural environments. *J. Environ. Psychol.* 65, 101328. doi:10.1016/j.jenvp.2019.101328, https://doi.org/.
- Minoshima, S., Giordani, B., Berent, S., Frey, K.A., Foster, N.L., Kuhl, D.E., 1997. Metabolic reduction in the posterior cingulate cortex in very early Alzheimer's disease. *Ann. Neurol.* 42, 85–94. doi:10.1002/ana.410420114, https://doi.org/.
- Morris, R., Pandya, D.N., Petrides, M., 1999. Fiber system linking the mid-dorsolateral frontal cortex with the retrosplenial/presubicular region in the rhesus monkey. *J. Comp. Neurol.* 407, 183–192.
- Nakao, T., Radua, J., Rubia, K., Mataix-Cols, D., 2011. Gray matter volume abnormalities in ADHD: voxel-based meta-analysis exploring the effects of age and stimulant medication. *Am. J. Psychiatry* 168, 1154–1163.
- Papez, J.W., 1937. A proposed mechanism of emotion. *Arch. Neurol. Psychiatry* 38, 725–743.
- Park, B.-J., Tsunetsugu, Y., Kasetani, T., Hirano, H., Kagawa, T., Sato, M., Miyazaki, Y., 2007. Physiological effects of shinrin-yoku (taking in the atmosphere of the forest)—using salivary cortisol and cerebral activity as indicators—. *J. Physiol. Anthropol.* 26, 123–128.
- Parvizi, J., Van Hoesen, G.W., Buckwalter, J., Damasio, A., 2006. Neural connections of the posteromedial cortex in the macaque. *Proc. Natl. Acad. Sci.* 103 (5), 1563–1568.
- Pelli, D.G., 1997. The VideoToolbox software for visual psychophysics: transforming numbers into movies. *Spat. Vis.* 10, 437–442. doi:10.1163/156856897X00366, https://doi.org/.
- Pierce, K., Haist, F., Sedaghat, F., Courchesne, E., 2004. The brain response to personally familiar faces in autism: findings of fusiform activity and beyond. *Brain* 127, 2703–2716.
- Pol, H.E.H., Schnack, H.G., Mandl, R.C., van Haren, N.E., Koning, H., Collins, D.L., Evans, A.C., Kahn, R.S., 2001. Focal gray matter density changes in schizophrenia. *Arch. Gen. Psychiatry* 58, 1118–1125.
- Roebroeck, A., Formisano, E., Goebel, R., 2005. Mapping directed influence over the brain using Granger causality and fMRI. *Neuroimage* 25, 230–242.
- Rosenbaum, R.S., Ziegler, M., Winocur, G., Grady, C.L., Moscovitch, M., 2004. "I have often walked down this street before": fMRI studies on the hippocampus and other structures during mental navigation of an old environment. *Hippocampus* 14, 826–835.
- Schroeder, H.W., 2011. Does beauty still matter? Experiential and utilitarian values of urban trees. In: *Trees, People and the Built Environment*. Proceedings of the Urban Trees Research Conference; 2011 April 13-14, Edgbaston, Birmingham, UK. Institute of Chartered Foresters, pp. 159–165 159-165.
- Schurger, A., 2009. A very inexpensive MRI-compatible method for dichoptic visual stimulation. *J. Neurosci. Methods* 177, 199–202.
- Serences, J.T., 2004. A comparison of methods for characterizing the event-related BOLD timeseries in rapid fMRI. *Neuroimage* 21, 1690–1700.
- Small, D.M., Zatorre, R.J., Dagher, A., Evans, A.C., Jones-Gotman, M., 2001. Changes in

- brain activity related to eating chocolate from pleasure to aversion. *Brain* 124, 1720–1733. doi:10.1093/brain/124.9.1720, <https://doi.org/>.
- Suzuki, W.L., Amaral, D.G., 1994. Perirhinal and parahippocampal cortices of the macaque monkey: cortical afferents. *J. Comp. Neurol.* 350, 497–533.
- Tang, I.-C., Tsai, Y.-P., Lin, Y.-J., Chen, J.-H., Hsieh, C.-H., Hung, S.-H., Sullivan, W.C., Tang, H.-F., Chang, C.-Y., 2017. Using functional magnetic resonance imaging (fMRI) to analyze brain region activity when viewing landscapes. *Landsc. Urban Plan.* 162, 137–144.
- Taylor, A.F., Kuo, F.E., Sullivan, W.C., 2002. Views of nature and self-discipline: evidence from inner city children. *J. Environ. Psychol.* 22, 49–63. doi:10.1006/jevp.2001.0241, <https://doi.org/>.
- Thomson, M.G., 1999. Visual coding and the phase structure of natural scenes. *Netw. Comput. Neural Syst.* 10, 123–132.
- Thomson, M.G., Foster, D.H., Summers, R.J., 2000. Human sensitivity to phase perturbations in natural images: a statistical framework. *Perception* 29, 1057–1069. doi:10.1068/p2867, <https://doi.org/>.
- Tost, H., Reichert, M., Braun, U., Reinhard, I., Peters, R., Lautenbach, S., Hoell, A., Schwarz, E., Ebner-Priemer, U., Zipf, A., 2019. Neural correlates of individual differences in affective benefit of real-life urban green space exposure. *Nat. Neurosci.* 22, 1389–1393.
- Ulrich, R., 1984. View through a window may influence recovery from surgery. *Science* 224, 420–421. doi:10.1126/science.6143402, <https://doi.org/>.
- Ulrich, R.S., 1981. Natural versus urban scenes: some psychophysiological effects. *Environ. Behav.* 13, 523–556. doi:10.1177/0013916581135001, <https://doi.org/>.
- Van den Berg, A.E., Hartig, T., Staats, H., 2007. Preference for nature in urbanized societies: stress, restoration, and the pursuit of sustainability. *J. Soc. Issues* 63, 79–96.
- Van der Schaaf, van A., van Hateren, J., 1996. Modelling the power spectra of natural images: statistics and information. *Vision Res.* 36, 2759–2770.
- Vann, S.D., Aggleton, J.P., Maguire, E.A., 2009. What does the retrosplenial cortex do? *Nat. Rev. Neurosci.* 10, 792–802.
- Vogt, B.A., Pandya, D.N., 1987. Cingulate cortex of the rhesus monkey: II. Cortical afferents. *J. Comp. Neurol.* 262 (2), 271–289.
- von Dawans, B., Kirschbaum, C., Heinrichs, M., 2011. The trier social stress test for groups (TSST-G): a new research tool for controlled simultaneous social stress exposure in a group format. *Psychoneuroendocrinology* 36, 514–522. doi:10.1016/j.psyneuen.2010.08.004, <https://doi.org/>.
- Wilkins, A.J., Andermann, F., Ives, J., 1975. Stripes, complex cells and seizures. An attempt to determine the locus and nature of the trigger mechanism in pattern-sensitive epilepsy. *Brain J. Neurol.* 98, 365–380. doi:10.1093/brain/98.3.365, <https://doi.org/>.
- Wolbers, T., Büchel, C., 2005. Dissociable retrosplenial and hippocampal contributions to successful formation of survey representations. *J. Neurosci.* 25, 3333–3340.